Convective Burning of Gaseous Fuel Pockets and Supercritical Droplets

J. DAOU and B. ROGG*

Lehrstuhl für Strömungsmechanik, Institut für Thermo- und Fluiddynamik, Ruhr-Universität, D-44780 Bochum, Germany

The present paper is concerned with combustion of an initially spherical kernel of cold fuel, which in a hot oxidizing atmosphere is suddenly put into motion. The investigations are within the framework of an axisymmetric geometry and the flame-sheet model. After a brief description of the aerodynamics of the burning process, including deformation and breakup of the fuel kernel, attention is focused on the study of the combustion time t'_{comb}, which *by definition* is the time required to consume practically all the fuel. First, the case of zero heat release is addressed. It is found that—due to deformation and straining of isoscalar surfaces—the direct dependence of the combustion time on the magnitude of the diffusivity of heat and matter decreases rapidly as the Reynolds number, Re, is increased. In particular, the combustion time t'_{comb} becomes independent of the magnitude of the diffusivity as soon as the Reynolds number exceeds a few hundred. In this high-Re regime, t'_{comb} is found to be proportional to the convective time t'_{conv} multiplied by the square root of the density ratio, Eq. 17. Next, the influence of heat release on the combustion time is studied. It is found that at high Reynolds numbers the combustion time increases with increasing heat release. This increase is found to be essentially due to the decrease of the scalar gradients, which in turn is caused by the gas expansion due to heat release. Furthermore, the effect of heat release on the vorticity distribution is studied, and the relative importance of baroclinicity and gas expansion on the vorticity production is assessed. Finally, the influence of the stoichiometry of the reaction on the combustion time is briefly discussed.

NOMENCLATURE

a'_0	initial radius of fuel kernel
c'_p	specific heat capacity of mixture at constant pressure
e	elongation parameter; see Eq. 9
F	fuel
m'_F	instantaneous total mass of fuel; see Eq. 8
Ox	oxidizer
p'	pressure
p	nondimensional pressure ($= p'/(\rho'_\infty U'^2_0)$)
P	products of chemical reaction
Pe	Peclet number ($= a'_0 U'_0/\kappa'_\infty = t'_{diff}/t'_{conv}$)
Pr	Prandtl number ($= \nu'_\infty/\kappa'_\infty$)
q'	heat of reaction per unit mass of fuel
q	nondimensional heat of reaction ($= q'/(c'_p T'_\infty)$)
Re	Reynolds number ($= a'_0 U'_0/\nu'_\infty$)
r_{fl}	nondimensional average flame radius
T'	temperature
T	nondimensional temperature ($= T'/T'_\infty$)
t'	time
t'_{conv}	convective time ($= a'_0/U'_0$)
t'_{diff}	diffusive time ($= a'^2_0/\kappa'_\infty$)
t'_{comb}	combustion time
t	nondimensional time ($= t'/t'_{conv}$)
U'_0	initial velocity of the fuel kernel
W'_0	deformation velocity of the fuel kernel
$\mathbf{v}$	nondimensional velocity ($= \mathbf{v}'/U'_0$)
Z	mixture fraction
Z_{st}	stoichiometric value of the mixture fraction

Greek Symbols

ϵ	temperature ratio ($= T'_\infty/T'_0$)
ϵ^{-1}	density ratio ($= \rho'_0/\rho'_\infty$)
κ'	diffusivity of heat and matter
ν'	kinematic viscosity (= diffusivity of momentum)
ν	stoichiometric coefficient; see Eq. 1
ρ'	density
ρ	nondimensional density ($= \rho'/\rho'_\infty$)

*Corresponding author.
Current address of J. Daou: Dpto. Motopropulsion y Termofluidinamica, Universidad Polytecnica de Madrid, E.T.S.I. Aeronauticos, Pl. Cardenal Cisneros 3, 28040 Madrid, Spain.

COMBUSTION AND FLAME 115:145–157 (1998)

Published by Elsevier Science Inc.
0010-2180/98/$19.00
PII S0010-2180(97)00354-4

τ nondimensional combustion time ($= t'_{comb}/t'_{conv}$)
ω nondimensional vorticity ($= \omega' a'_0/U'_0$)
Δ nondimensional Laplace operator ($= a'^2_0 \Delta'$)
∇ nondimensional gradient operator ($= a'_0 \nabla'$)

Subscripts

F values of fuel kernel
0 initial values of fuel kernel
∞ values in the far field

Superscript

$'$ identifies a dimensional quantity

INTRODUCTION

In nonpremixed combustion, the occurrence of inhomogeneities moving relative to the surrounding gas is a common phenomenon. For instance, in diesel engines or rocket motors, concentration and density inhomogeneities are generated by injecting fuel droplets into a hot oxidizing atmosphere. Although the results of the present study could be placed in a more general framework, herein we concentrate on aspects relevant to supercritical droplet combustion. (Thus, we assume that in the vicinity of the original liquid–gas interface supercritical conditions prevail and that, therefore, this region can no longer be viewed as a discontinuity in thermodynamic properties.) Because of its particular relevance to high-pressure combustion, where both pressure and temperature typically take values well beyond the critical values of the fuel, the supercritical regime and the conditions under which it is attained have been the subject of a number of investigations; see, for example, Refs. [1–8].

Available studies of droplet vaporization and combustion fall into two categories. In the first category, which is by far the larger, the *assumption of spherical symmetry* has been adopted under both subcritical and supercritical conditions, thus neglecting the influence of nonuniform relative motion between droplet and ambient gas. In this category, recent studies have devoted special attention to the thermodynamic treatment of the liquid–gas interface, a particularly important point for transcritical droplet behavior. To this end, cubic equations of state have been used to determine the composition at both sides of the interface and mixture critical points [7]. Furthermore, for the spherically symmetrical case, analytical and numerical studies exclusively devoted to the supercritical regime have been conducted [1, 4, 9].

Studies in the second category have considered *droplets moving relative to the ambiance with significant Reynolds numbers*. With only a few exceptions, in these studies the important assumption has been adopted that surface tension effects are sufficiently strong to maintain a spherical droplet shape: the Weber number has been taken as small. Under this restriction, the gasification rate at the front of the droplet surface has been evaluated on the basis of a boundary-layer type analysis, which, typically, has led to a square-root dependence of the droplet lifetime on a characteristic diffusion coefficient. Of course, the assumption of a small Weber number is no longer acceptable under near-critical conditions where surface tension effects are vanishingly small. Therefore, for large values of the Weber number, substantial droplet deformation occurs, which can be expected to play an important role in mixing and combustion. In this context, the present study can be viewed as representing the limit of infinite Weber number.

Pure mixing in the supercritical regime, with combustion disregarded, has been addressed by Lee et al. [10] in the framework of a constant density assumption. In their paper, the deformation process of an initially spherical kernel of fuel in a hot oxidizing environment is described, and the enhancement of mixing is inferred without detailed examination of its dependence on parameters. For subcritical vaporization, a complete model, including two-phase flow, high-pressure thermodynamics and effects of finite surface tension, has been proposed and successfully treated numerically by Deng et al. [11]. Because of the simultaneous inclusion in the model of a variety of complex physical phenomena, the study of these authors can be considered as a pioneering one. Recently, dropping the constant density assumption, Daou and Haldenwang [12] have investigated the physi-

cally similar problem of the heating a puff of cold fluid injected into a hot gas, particularly focusing attention on the functional dependence of the heating time on parameters. In part, the present work can be considered as an extension of the study in [12] to combustion situations.

The organization of the present paper is as follows. First, the physical model is presented. Here the governing equations are given in nondimensional form, and the simplifying assumptions on thermodynamic properties and transport properties are discussed. Then, using cylindrical coordinates, the governing equations are solved numerically. In the subsequent presentation of results, we first consider a typical case characterized by substantial droplet deformation. The aerodynamic features of the burning process are described, and useful temporal quantities are introduced. This is followed by the central issue of the paper, namely, the study of the combustion time. First, the case of zero heat release is considered, for which the asymptotic scaling laws governing the combustion time in the limit of small and large Reynolds number, respectively, are established. Then, the influence of heat release is analyzed. In particular, in this context the vorticity distribution is examined. Finally, the influence of the stoichiometry of the reaction on the combustion time is briefly discussed.

MODEL

The evolution of an initially spherical kernel of fuel, which in a hot oxidizing atmosphere is suddenly set into motion, is considered. Axisymmetric flow at low Mach numbers is assumed. The thermal conductivity, the heat capacity at constant pressure, the molecular weight, and the dynamic viscosity, all of the gas mixture, as well as the products of the density with the individual species diffusion coefficients are taken as constants. The Burke–Schumann flame-sheet model is adopted. Thus, equal diffusivities of heat and matter are assumed, and combustion is described by a single irreversible and infinitely fast one-step reaction of the form

$$F + \nu Ox \rightarrow P \tag{1}$$

where F denotes the fuel, Ox the oxidizer, and P the products. The stoichiometric coefficient ν represents the moles of oxidizer consumed per mole of fuel. With these assumptions, the governing equations can be written in nondimensional form as

$$\frac{\partial \rho}{\partial t} + \nabla \cdot (\rho \mathbf{v}) = 0 \tag{2}$$

$$\rho \frac{\partial \mathbf{v}}{\partial t} + \rho \mathbf{v} \cdot \nabla \mathbf{v} = -\nabla p + \mathrm{Re}^{-1} \Delta \mathbf{v} \tag{3}$$

and

$$\rho \frac{\partial Z}{\partial t} + \rho \mathbf{v} \cdot \nabla Z = (\mathrm{RePr})^{-1} \Delta Z \tag{4}$$

Here ∇ and Δ denote the nondimensional gradient and Laplace operator, respectively, Z is the mixture fraction, Re is the Reynolds number, and Pr is the Prandtl number. Nondimensionalization involving the initial kernel radius, the initial kernel velocity, and the density in the far field has been used; for details, the Nomenclature should be consulted. In Eq. 3 the gradient of a term involving the product of dynamic viscosity and dilatation has been lumped into the pressure gradient [13].

The density ρ is assumed to obey the ideal-gas equation of state; it is easily shown that under the above assumptions it is linked to the mixture fraction Z by

$$\rho = \begin{cases} [1 - (1 - \epsilon) Z + qZ]^{-1} & \text{for} \quad Z \le Z_{st} \\ \left[1 - (1 - \epsilon) Z + q \dfrac{Z_{st}(1 - Z)}{(1 - Z_{st})} \right]^{-1} & \text{for} \quad Z \ge Z_{st} \end{cases} \tag{5}$$

Here Z_{st} denotes the stoichiometric value of the mixture fraction; ϵ is the ratio

$$\epsilon \equiv \frac{T'_\infty}{T'_0} \tag{6}$$

of the initial temperature of the kernel, T'_0, to the temperature in the far field, T'_∞. The reciprocal of ϵ, ρ'_0/ρ'_∞, is the *density ratio*. The quantity q is the nondimensional heat of reaction per unit mass of fuel,

$$q \equiv \frac{q'}{c'_p T'_\infty} \tag{7}$$

It characterizes the amount of heat release.

The initial conditions at $t = 0$ correspond to a spherical kernel of fuel with a nondimensional radius of unity, which is placed around the origin. Inside the kernel, the initial values $Z = 1$ and $\mathbf{v} = \mathbf{e}_x$ are adopted. Here $\mathbf{e}_x$ is the unit vector in the axial direction. Outside the kernel, the initial conditions are $Z = 0$ and $\mathbf{v} = \mathbf{0}$. The boundary conditions correspond to a stagnant hot atmosphere at infinity, which contains oxidizer but no fuel. Thus far from the kernel, at any instant the conditions $Z = 0$ and $\mathbf{v} = \mathbf{0}$ apply. Note that by virtue of Eq. 5, initially $\rho = \epsilon^{-1}$ inside the kernel and $\rho = 1$ outside it. Similarly, at any instant of time, far from the kernel $\rho = 1$.

The problem is specified in terms of five nondimensional parameters: the Reynolds number Re, the Prandtl number Pr, the density ratio ϵ^{-1}, the stoichiometric mixture fraction Z_{st}, and the heat-release parameter q. It is convenient to introduce the instantaneous total mass m'_F of fuel,

$$m'_F = m'_F(t') = \int_{V'} \frac{Z - Z_{st}}{1 - Z_{st}} \rho' \, \mathrm{d}V' \tag{8}$$

which will be used to characterize the overall combustion time. In Eq. 8, V' denotes the volume of the kernel inside the iso-surface $Z = Z_{st}$.

Numerical Considerations

Equations 2–4, in cylindrical coordinates, are discretized using a finite volume approach. The resulting difference equations are then solved with a multigrid method [14, 15]. The extent of the computational domain in both the axial and radial direction is large compared to the initial radius of the kernel. In each direction, the extent of the domain was at least 40 times the initial kernel radius, dimensions which numerical tests showed to be adequate for all cases considered.

The grid used in the computations was a nonuniform tensor–product grid with typically 400×200 grid points. To ensure grid independence of the results, some cases were checked with grids of up to 600×300 points. The grid points were concentrated in regions of strong spatial activity of the dependent variables, with the aim of equidistributing the local spatial truncation error. After each time step, the solution of the governing equations was remapped onto the domain such that the flame remained located approximately at the origin of the coordinate system.

The results to be presented below do not show the full computational domain but only a small portion of it. Due to the huge amount of computed data, the temporal results were not stored at all grid points but only at selected ones.

RESULTS AND DISCUSSION

First, we consider a typical case corresponding to Re = 100, for which the flame and the fuel kernel experience substantial deformation. This provides a qualitative description of the aerodynamic features of the problem and introduces some temporal quantities characterizing the history of kernel burning. Second, we turn to the central issue of this paper, namely, the determination of the combustion time. To better understand the influence of heat release, we proceed in two steps: first, the case of zero heat release, $q = 0$, for which we establish the asymptotic scaling laws, and, second, the general case of nonzero heat release, $q > 0$. Finally, the effect of stoichiometry on the numerical results is briefly described.

A Typical Case with Substantial Kernel Deformation

A first appreciation of the hydrodynamics and of the evolution of the burning process is presented for Re = 100, Pr = 1, $\epsilon = 0.1$, $Z_{st} = 0.8$, and $q = 2$. Figure 1 shows four sequential pictures for $t = 0.2$, 4, 10, and 16. The

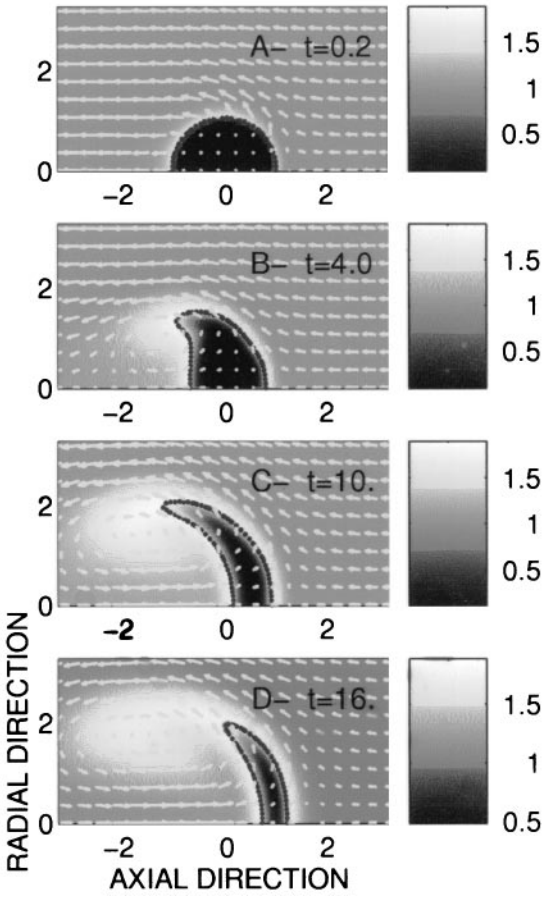

Fig. 1. Deformation and burning of the fuel kernel for Re = 100, Pr = 1, $q = 2$, $\epsilon = 0.1$, and $Z_{st} = 0.8$. Diffusion flame represented by dotted mixture fraction contour, $Z = Z_{st}$. Arrows visualize velocity field relative to a frame moving with the average velocity of the kernel. Colors describe the nondimensional temperature field. Times $t = 0.2$, 4, 10, and 16, sequentially.

instantaneous flame position is indicated by the dotted line, which corresponds to the mixture fraction contour $Z = Z_{st}$; colors describe the nondimensional temperature field T, whereas arrows visualize the nondimensional velocity field relative to a frame moving with a suitably defined average velocity of the kernel. It is seen that the kernel experiences a substantial deformation, essentially a stretching in the direction perpendicular to the flow. This deformation has been attributed [16, 17] to the combined action of nonuniform pressure distribution and vorticity. The velocity field indicates the presence of a large circulation region at the back of the deformed kernel, with a vorticity core close to its rim. The flame roll-up is seen to be quite limited in this case; this roll-up is—as will be discussed below—more pronounced at higher Reynolds numbers and lower rates of heat release.

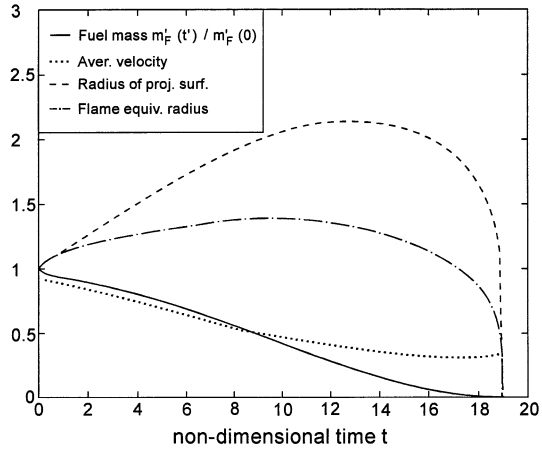

Fig. 2. Total fuel mass (solid line), average kernel velocity (dotted line), equivalent flame radius (dashed dotted line), and radius of flame area projected onto plane perpendicular to the symmetry axis (dashed line) vs. time. All quantities are nondimensional. Parameter values as for Fig. 1.

Figure 2 illustrates the evolution of four temporal quantities: the total fuel mass, defined in Eq. 8, the mass-weighted average velocity of the fuel-containing region (the region surrounded by the flame), the radius of the flame area projected onto a plane perpendicular to the axial direction, and the flame equivalent radius. All quantities are normalized with their respective initial values. The equivalent radius is defined as the radius of a sphere having the same volume as the fuel-containing region. Examination of these quantities reveals that the fuel mass decreases almost linearly with time, that the average velocity remains substantial during the whole lifetime of the kernel, and that the kernel deformation continually increases. The extent of deformation, which alternatively may be termed *nonsphericity*, can conveniently be quantified by a nondimensional elongation parameter e, defined as

$$e = \frac{\text{radius of projected area}}{\text{equivalent radius}} \tag{9}$$

In terms of e, spherical flames are characterized by $e = 1$, flames stretched in the radial direction by $e > 1$, and flames stretched in the axial direction by $e < 1$.

Determination of the Combustion Time

A convenient way to characterize the global intensity of combustion is to plot the instantaneous total fuel mass as a function of time, as in Fig. 2, and to estimate from such a plot the time after which *practically* all fuel has been consumed. This time is referred to as the *combustion time*, t'_{comb}. It should not to be confused with the combustion *rate*, which can be defined, for instance, as the slope of a graph of the instantaneous total fuel mass vs. time. Understanding of the combustion time is the key issue of the present paper and, in particular, of this section.

Preliminary Dimensional Considerations

The nondimensional combustion time, τ, can be expressed in terms of the governing parameters by

$$\tau = \Psi(\mathrm{Re}, \mathrm{Pr}, \epsilon, q, Z_{st}) \tag{10}$$

Obtaining detailed knowledge of the function Ψ is a formidable task that will not be attempted here. Simplifications are achieved by taking a single selected value of the stoichiometric mixture fraction and by studying first the case $q = 0$ without heat release. Such simplifications make it possible to appreciate the variation of τ in terms of the other parameters. Variations of the form

$$\tau = \Phi(\mathrm{Re}, \mathrm{Pe}, \epsilon) \tag{11}$$

are considered with the Peclet number, $\mathrm{Pe} = \mathrm{Pr} \cdot \mathrm{Re}$.

It is important to investigate the asymptotic behavior of the function Φ for large values of Re and Pe and to examine the permissibility of dropping the dependence on these parameters. It will be shown that this is indeed permissible as soon as the values of these parameters exceed a few hundred and that then τ assumes the simple functional form

$$\tau = \Pi(\epsilon) = \Phi(\infty, \infty, \epsilon) \tag{12}$$

It will be shown below, Eq. 16, that the function Π is proportional to the square root of the density ratio,

$$\tau \propto \sqrt{\epsilon^{-1}} \tag{13}$$

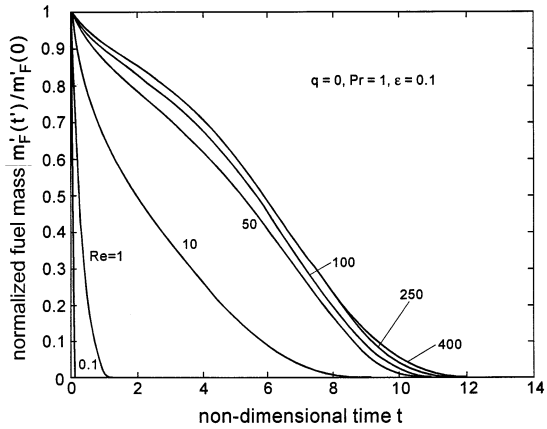

Fig. 3. Normalized total fuel mass vs. nondimensional time for different values of Re for $q = 0$, $\epsilon = 0.1$, $Z_{st} = 0.8$, and $\mathrm{Pr} = 1$.

for high Pe. In the opposite low Reynolds number limit, as expected (not shown here), the asymptotic behavior of τ is

$$\tau \propto \epsilon^{-1}\,\mathrm{Pe} \tag{14}$$

for low Pe. In terms of dimensional quantities, this represents the well-known result

$$t'_{comb} \propto \frac{\rho'_0}{\rho'_\infty}\, t'_{diff} \tag{15}$$

for low Pe for droplet vaporization and combustion in a stagnant environment, even in the supercritical case [1].

Combustion without Heat Release

The dependence of the combustion time on Re, Pr, and ϵ is considered for zero heat release, $q = 0$, and for a fixed value of the stoichiometric mixture fraction Z_{st} of 0.8. The sensitivity of the results to the value of Z_{st} is discussed later. These results are summarized in Figs. 3–5, where the total fuel mass, initialized by its initial value, is plotted against nondimensional time for different values of Re. Figure 3, for $\mathrm{Pr} = 1$ and $\epsilon = 0.1$, clearly shows the dependence of the fuel mass on Re to become increasingly weak as this parameter increases. This suggests that Reynolds number similarity applies (the dependence on Re can be dropped) as soon as the Peclet number (in this case equal to Re because $\mathrm{Pr} = 1$) is larger than about 200. The same conclusion can also be reached from Fig.

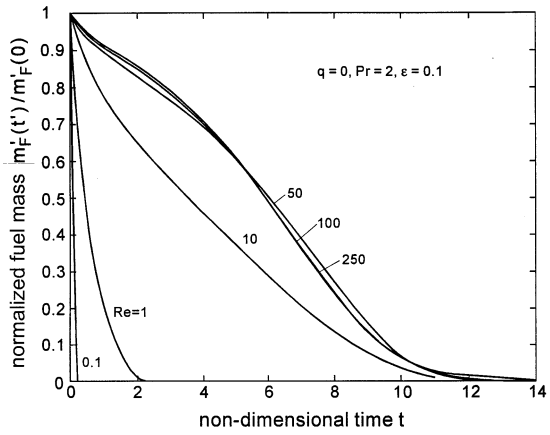

Fig. 4. As Fig. 3, but with Pr = 2.

4, which is for Pr = 2 and $\epsilon = 0.1$. Comparison of Figs. 3 and 4 also shows that the dependence on Pr can be dropped, provided Pe is sufficiently large. Finally, when compared to Fig. 4, Fig. 5, for Pr = 1 and $\epsilon = 0.05$, displays the influence of the density ratio ϵ^{-1} on the combustion time τ, namely, a linear dependence at low Reynolds numbers and a square root dependence at high Reynolds numbers. Finally, the asymptotic behavior observed at high Re is further stressed in Fig. 6, where five curves are plotted. Note that (e) is identical to (d) but with the time divided by $\sqrt{2}$. The curves corresponding to (a) to (c) and (e) collapse to a single curve exhibiting the independence of the normalized total fuel mass on both Pr and Re as well as the square root dependence on the density ratio.

At sufficiently high values of Pe, the nondi-

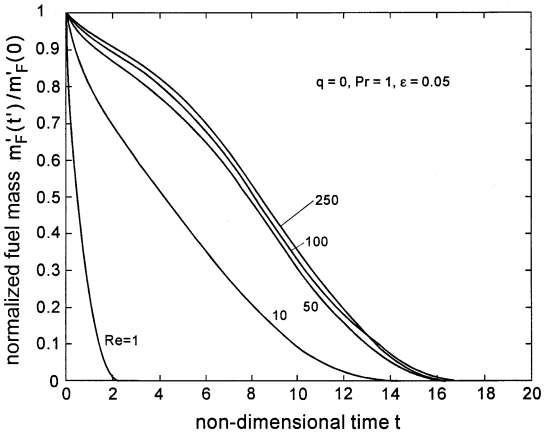

Fig. 5. As Fig. 3, but with $\epsilon = 0.05$.

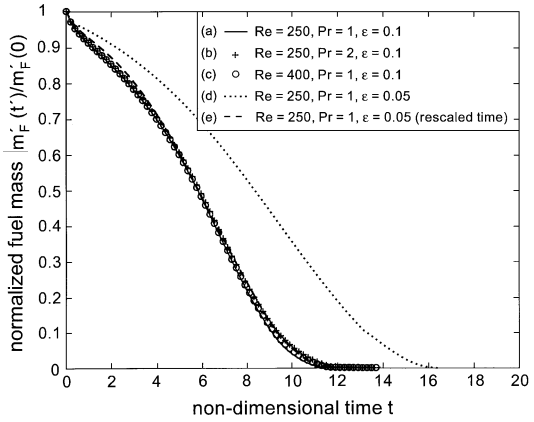

Fig. 6. Five curves plotted vs. time, all for $q = 0$ and $Z_{st} = 0.8$. (a) Re = 250, Pr = 1, and $\epsilon = 0.1$, (b) Re = 250, Pr = 2, and $\epsilon = 0.1$, (c) Re = 400, Pr = 1, and $\epsilon = 0.1$, (d) Re = 250, Pr = 1, and $\epsilon = 0.05$, and (e) is the same as (d) but with the time divided by $\sqrt{2}$. The collapse of curves (a), (b), (c), and (e) confirms the asymptotic form of the kernel lifetime given by Eq. (16).

mensional combustion time takes the asymptotic form

$$\tau = C\sqrt{\epsilon^{-1}} \tag{16}$$

for high Pe, where the value of the constant C depends on Z_{st}. In dimensional form, with C replaced by the proportionality sign and with ϵ expressed in terms of the density ratio, Eq. 16 becomes

$$t'_{comb} \propto t'_{conv}\sqrt{\frac{\rho'_0}{\rho'_\infty}} \tag{17}$$

for high Pe, showing that the dimensional combustion time t'_{comb} is proportional to the convective time (based on initial kernel radius and velocity) multiplied by the square root of the density ratio. In particular, t'_{comb} does not depend on the coefficients of diffusion of mass and heat, κ_∞, and momentum, ν_∞. Nevertheless, it is informative to examine how diffusion of mass, heat, and momentum are manifest at high values of Re. This is illustrated in Figs. 7 and 8 for Re = 250 but with different values of Pr. The velocity fields are indistinguishable, and the evolution of the flame, represented by the isoscalar surface $Z = Z_{st}$, is almost identical in both cases except for a small-scale difference near the vortex core (compare the roll-up at time $t = 6$ in the two figures). If the viscosity is varied such that the Reynolds number remains

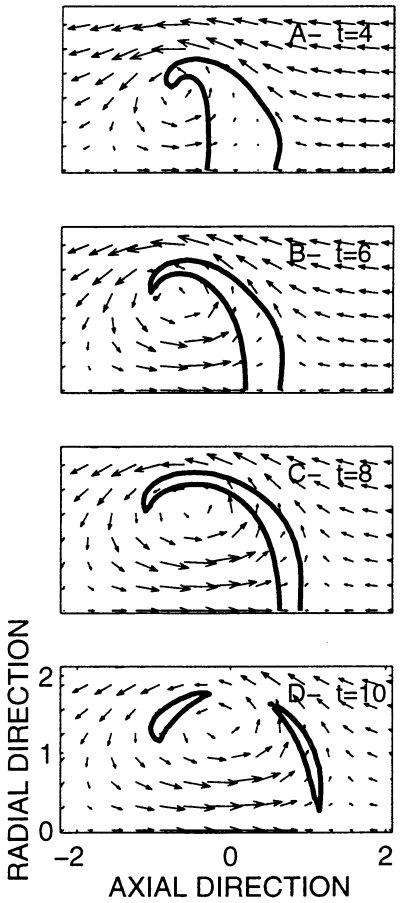

Fig. 7. Temporal sequence of pictures showing flame and velocity field at—from top to bottom—$t = 4$, 6, 8, and 10. Re = 250, $\epsilon = 0.1$, Pr = 1, $q = 0$, and $Z_{st} = 0.8$.

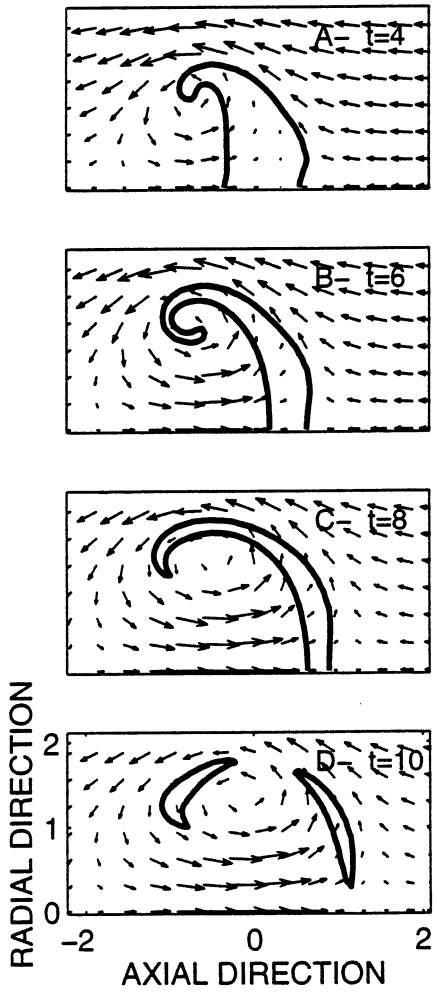

Fig. 8. As Fig. 7, but with Pr = 2.

large, even smaller differences are observed. This illustrates the independence of the gross characteristics of the flow on diffusive processes. If the combustion time is independent of the diffusion coefficient, then it is reasonable to expect that this time should be of the same order as a *deformation time* that characterizes the deformation of the fuel-containing region. The deformation time can be estimated as the ratio of the initial kernel radius and a typical deformation velocity, W'_0, say. Equating the order of magnitude of the dynamic pressure around the kernel, $\rho'_\infty U'^2_0$, with the order of magnitude of the dynamic pressure inside the kernel, $\rho'_0 W'^2_0$, yields the estimate $W'_0 = \epsilon^{1/2} U'_0$. The latter result leads, in nondimensional variables, to a nondimensional deformation time with the functional form of Eq. 16.

It is also straightforward to show with the aid of Figs. 3–5 that for low values of the Peclet number the asymptotic form of Eq. 14 holds.

Influence of Heat Release on Combustion Time and Vorticity

It is reasonable to expect that the above results for $q = 0$ will be approximately valid for the small heat-release situations frequently encountered when the gas surrounding the kernel is sufficiently hot. It now will be shown that the effects of heat release are *qualitatively quite different* for low and high Reynolds numbers. Although an increase in the value of q reduces the combustion time at low values of Re, it increases it at high values.

Shown in Fig. 9 is the normalized fuel mass

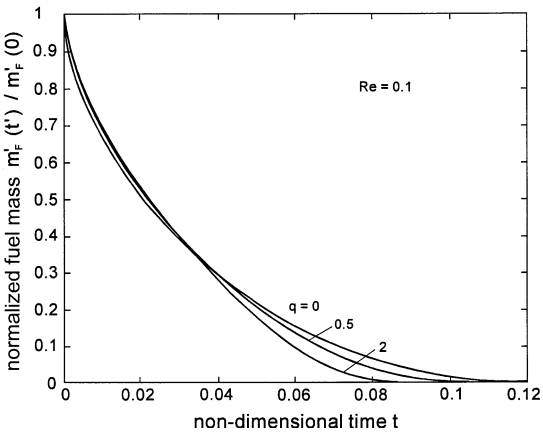

Fig. 9. Normalized total fuel mass vs. nondimensional time for different values of q for Re = 0.1, $\epsilon = 0.1$, $Z_{st} = 0.8$, and Pr = 1.

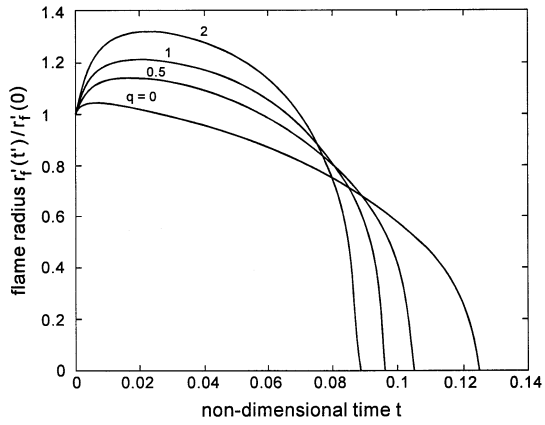

Fig. 11. Normalized flame radius vs. nondimensional time for different values of the q for Re = 0.1, $\epsilon = 0.1$, $Z_{st} = 0.8$, and Pr = 1.

vs. nondimensional time for different values of q at low Re, namely 0.1. Shown in Fig. 10 are the same results with Re = 100. Discussion focuses principally on the latter. For low Re, the combustion time decreases with increasing heat-release q, although for short times the combustion rate can be slightly higher for $q = 0$. This indicates an initially reduced fuel flux to the flame in the heat-release case, which can be traced to a higher gas expansion blowing the flame away from the kernel. The latter effect is illustrated in Fig. 11, where the flame radius is plotted vs. time for different values of q.

In contrast, Fig. 10 shows an increase in the combustion time with increases in q. This is because the heat release reduces the straining of scalar surfaces and hence the overall combustion rate, thereby increasing the combustion time. It is to be expected that the deformation of the fuel kernel and of the surrounding flame

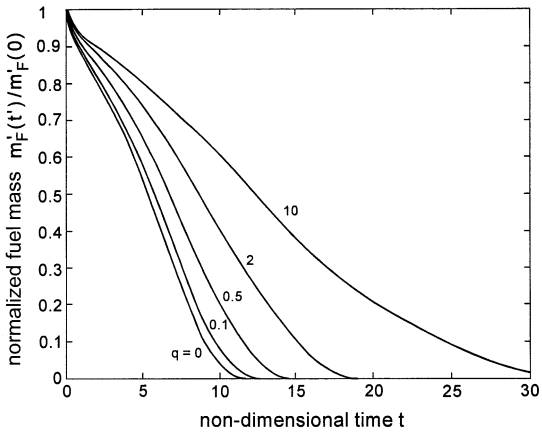

Fig. 10. As Fig. 9, but for Re = 100.

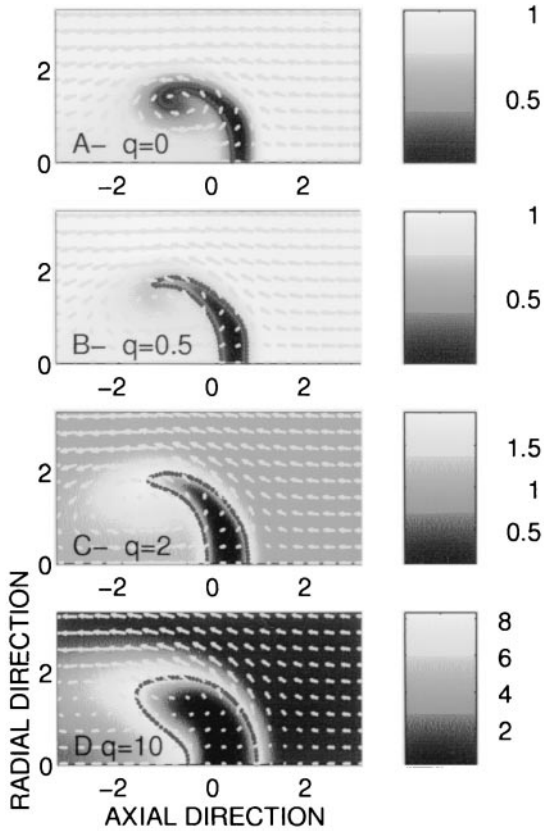

Fig. 12. Flame shape (dotted line) and temperature field (described by colors) at $t = 8$ for $q = 0$, 0.5, 2, and 10. Re = 100, $\epsilon = 0.1$, $Z_{st} = 0.8$, and Pr = 1.

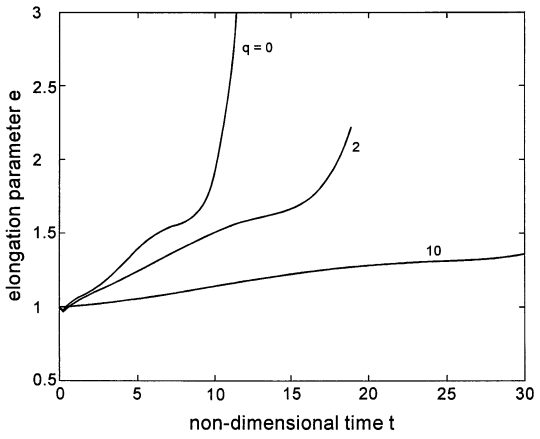

Fig. 13. Elongation parameter e vs. nondimensional time for $q = 0$, 2, and 10. Re = 100, $\epsilon = 0.1$, $Z_{st} = 0.8$, and Pr = 1.

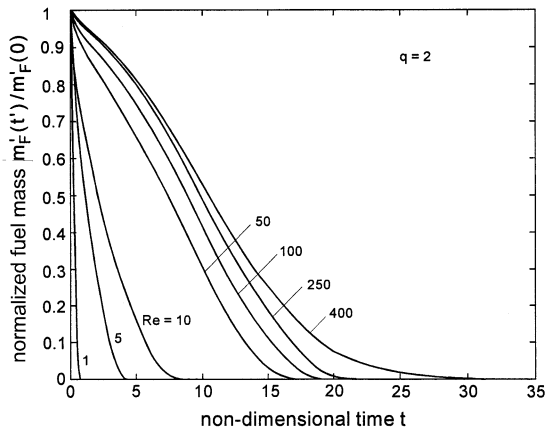

Fig. 14. Normalized total fuel mass vs. nondimensional time for different values of Re for $q = 2$, $\epsilon = 0.1$, $Z_{st} = 0.8$, and Pr = 1.

is diminished due to gas expansion as the heat release is increased. This is clearly illustrated in Fig. 12, which shows the flame shape and temperature field at $t = 8$ for $q = 0$, 0.5, 2, and 10. The flame roll-up is strongest for $q = 0$. More importantly, the flame and the fuel-containing region experience stretching in a direction essentially orthogonal to the symmetry axis, which becomes weaker with increasing q. This is illustrated further in Fig. 13, where the elongation parameter e is plotted against nondimensional time. Here higher values of e obtained for smaller values of q indicate an increasingly substantial deformation of the fuel kernel and the flame. They also provide a rough indication of the straining of scalar surfaces at least in the early stages of combustion where, in the high-Re case, the effect of diffusive processes on the overall behavior can be ignored.

The combustion time is examined for a fixed value of the heat release parameter, $q = 2$. Shown in Fig. 14 is the normalized instantaneous total mass of fuel as a function of nondimensional time for different values of Re. The dependence of the fuel mass on Re decreases as the latter is increased, although this is less pronounced than in the case $q = 0$. This can be attributed to the smaller deformation when heat release is present, which makes the direct contribution of diffusive effects (more specifically, the value of the diffusion coefficient) more important. Another factor, which also increases this contribution, is the decrease in the value of density (and thus in the conservation equations the magnitude of the convective terms compared to that of the diffusive terms) that accompanies heat release over large parts of the flow field. Shown in Fig. 15 are the same quantities as in Fig. 6, but for $q = 2$ instead of $q = 0$. From Fig. 15 it can be deduced that, even in this case with $q = O(1)$, for Peclet numbers somewhat higher than in the case $q = 0$, e.g., Pe $>$ 300, the asymptotic form given by Eq. 16 can be used as a good approximation.

Finally, the influence of heat release on the vorticity field is studied. Figure 12 shows flame roll-up to be strongest for $q = 0$. The axisymmetric vorticity transport equation reduces to

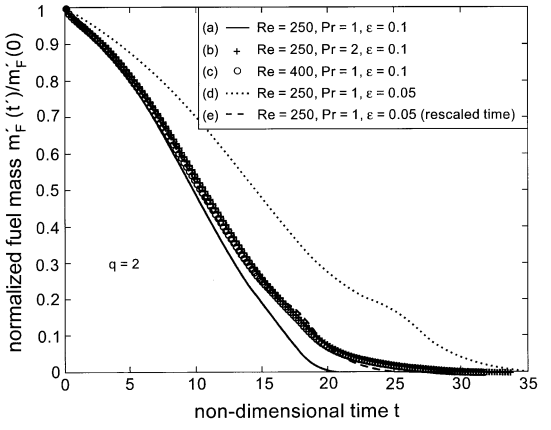

Fig. 15. As Fig. 6, but with $q = 2$.

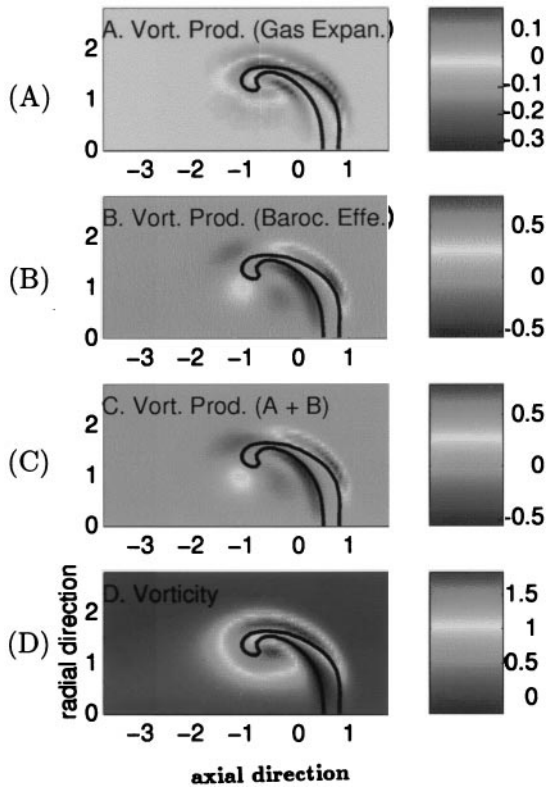

Fig. 16. Spatial distribution of: (a) vorticity production by gas expansion, (b) vorticity production by the baroclinic effect, (c) net vorticity production (sum of (a) + (b)), and (d) vorticity field; all for $q = 0$.

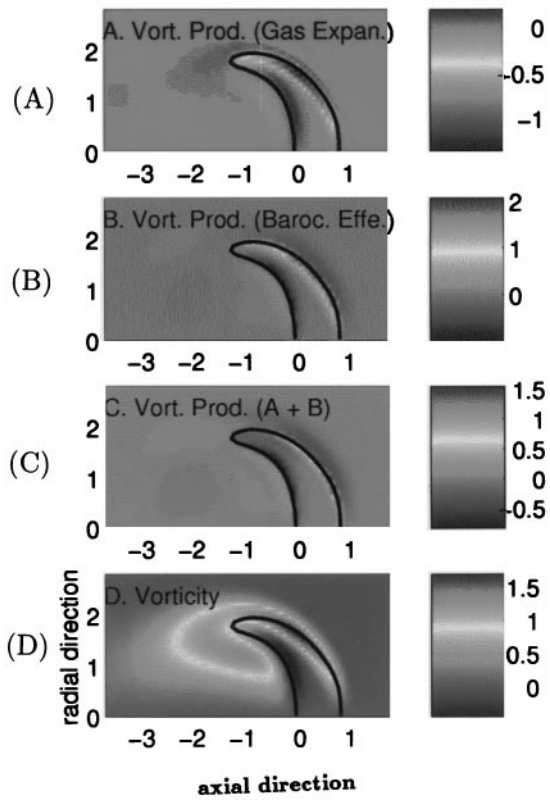

Fig. 17. As Fig. 16, but for $q = 2$.

$$\frac{\partial \omega}{\partial t} + \mathbf{v} \cdot \nabla \omega = -\omega \cdot (\nabla \cdot \mathbf{v}) + \frac{\nabla \rho \times \nabla p}{\rho^2} + \frac{1}{\mathrm{Re}} \Delta \omega \qquad (18)$$

On the right, the first term represents the production of vorticity by gas expansion, the second production by the baroclinic effect. To illustrate the way heat release affects vorticity, we plot in Figs. 16–18 the spatial distribution of four quantities: (a) vorticity production by gas expansion, (b) vorticity production by the baroclinic effect, (c) net vorticity production (sum of (a) + (b)), and (d) the vorticity field. The figures cover $q = 0$, 2, and 10, respectively.

For $q = 0$, Fig. 16, the vorticity production by the two terms in Eq. 18 is nonzero because the density distribution is initially nonuniform. The size of the region of *positive* vorticity production by gas expansion is comparable to that of the region with *negative* production by gas expansion. This is because, when heated, (expanding) fluid particles spin less intensively, whereas, when cooled, they spin more. With zero heat release, the flame does not contribute to the modification of this symmetric process. Gas expansion has only a small role compared to the baroclinic effect, which determines the net production of vorticity. The maximum vorticity occurs in a core around which flame roll-up takes place.

A comparison of Figs. 16(a), 17(a), and 18(a) shows how vorticity production by gas expansion is modified by heat release. The baroclinic effect is sensitive to the heat release as can be seen from Figs. 16(b), 17(b), and 18(b). The baroclinic term changes sign across the flame, a well-known phenomenon caused by the change in sign of the density gradient across a diffusion flame. The increase of the magnitude of the density gradient at both sides of the flame due to heat generation promotes both vorticity production at one side and vorticity destruction at the other. The essential action of the gas-

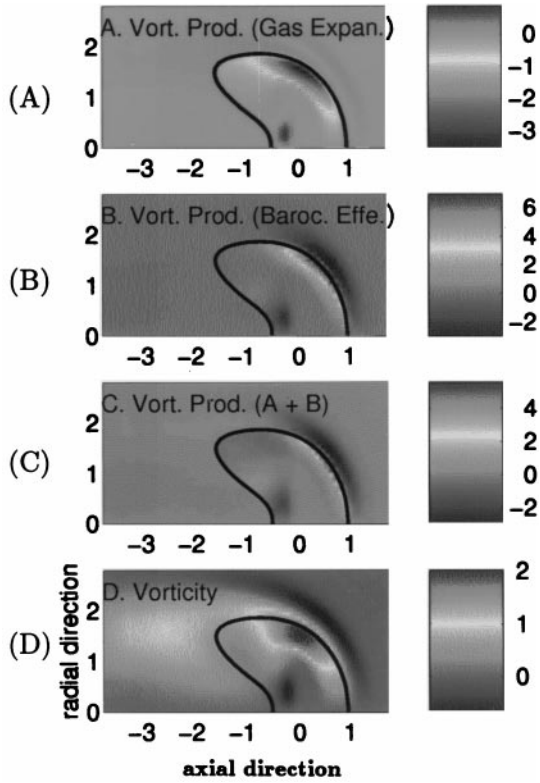

Fig. 18. As Fig. 16, but for $q = 10$.

expansion term in the vorticity transport equation is to decrease the magnitude and extent of positive vorticity production by baroclinicity.

Examination of the vorticity in Figs. 16(d), 17(d), and 18(d) shows the maximum value is slightly decreased for moderate heat release ($q = 2$) but can be increased for high values, such as $q = 10$. This local increase in vorticity is due to baroclinic vorticity production. The vorticity core responsible for flame roll-up is spread with increasing values of q and has a decreasing influence: it is hardly noticeable for $q = 10$. The vorticity spread is the clearest and most obvious effect of heat release, and it is also consistent with the decrease of the scalar gradients. To obtain a general idea about the overall effect of q on the vorticity, in Fig. 19 the volume average of vorticity over the fuel-containing region is plotted against time. The effect of *moderate* heat release on the reduction of the average vorticity is obvious.

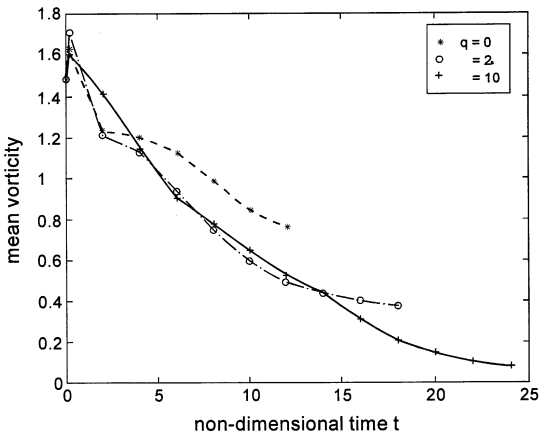

Fig. 19. Volume-averaged nondimensional vorticity over the fuel-containing region versus nondimensional time for cases of Figs. 16–18, respectively.

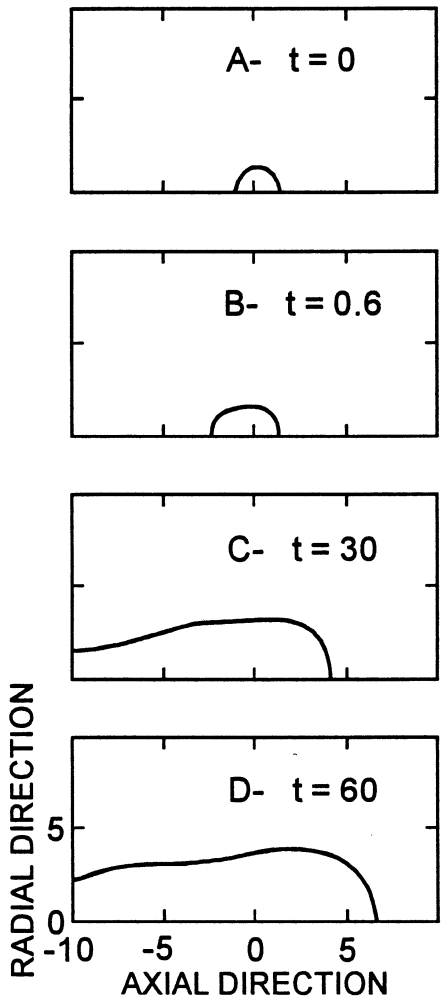

Fig. 20. Temporal sequence of pictures showing the evolution of a flame for $Z_{st} = 0.1$, $q = 2$, Re = 100, Pr = 1, and $\epsilon = 0.1$.

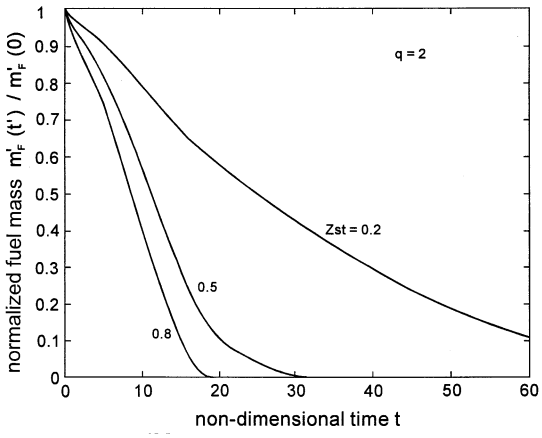

Fig. 21. Normalized total fuel mass vs. nondimensional time for $Z_{st} = 0.8$, 0.5, and 0.2. Values of the other parameters as in Fig. 20.

Effect of Stoichiometric Mixture Fraction Z_{st}

To complement the results presented above, we briefly discuss the influence of stoichiometry. The conclusions drawn above for $Z_{st} = 0.8$ can at least qualitatively be expected to extend to lower values of Z_{st}, for example, down to 0.4. For very low values of Z_{st}, much of the burning occurs far from the dense kernel. Figure 20 presents the flame contour for $Z_{st} = 0.1$, with $q = 2$ and Re = 100. As a consequence of the reduced straining of the flame associated with this broad combustion region, the combustion time is increased. That this indeed is the case is illustrated in Fig. 21, where the normalized instantaneous total mass of fuel is plotted against nondimensional time for different values of Z_{st}. It is seen that the combustion time is *substantially* increased if the value of Z_{st} becomes sufficiently small.

CONCLUSIONS

Burning of a dense fuel kernel moving relative to a hot oxidizing gas has been investigated within the framework of a flame-sheet combustion model. Axisymmetric flow conditions have been assumed. The deformation features of flame and kernel have been described and a detailed analysis of the combustion rate has been provided. The influence of heat release on the vorticity distribution has been studied.

For zero heat release, it has been shown that the influence of the magnitude of the diffusion coefficient on the combustion time disappears as soon as the Reynolds number, Re, exceeds a few hundred and that a square root dependence of the combustion time on the density ratio is obtained. The zero heat release results have been shown to hold also for moderate heat release.

For combustion with more than moderate heat release, it was found that at low Re the combustion time decreases with increasing rates of heat release, q, whereas for sufficiently large values of Re it increases with increasing q.

The present study was supported by the Commission of the European Communities within the framework of the Programme "Gravity Dependent Phenomena in Combustion."

REFERENCES

1. Sanchez-Tarifa, C., Crespo, A., and Fraga, E., *Astron. Acta* 17:685 (1972).
2. Shuen, J. S., Yang, V., and Hsiao, C. C., *Combust. Flame* 89:299 (1992).
3. Yang, V., Lin, N., and Shuen, J. S., *Combust. Sci. Technol*. 97:247 (1984).
4. Daou, J., Haldenwang, P., and Nicoli, C., *Combust. Flame* 101:153 (1995).
5. Haldenwang, P., Nicoli, C., and Daou, J., *Int. J. Heat Mass Transfer* 39:3453 (1996).
6. Nicoli, C., Haldenwang, P., and Daou, J., *Combust. Sci. Technol*. 112:55 (1996).
7. Umemura, A., and Shimada, Y., (1997) *Twenty-Sixth Symposium (International) on Combustion*, The Combustion Institute, Pittsburgh, p. 1621.
8. Umemura, A., and Jia, W., in *Modelling in Combustion Science* (J. D. Buckmaster and T. Takeno, Eds.), Springer-Verlag, Berlin, 1995, p. 237.
9. Spalding, D. B., *ARS J*. 29:828 (1959).
10. Lee, H. S., Fernandez-Pello, A. C., Corcos, G. M., and Oppenheim, A. K., *Combust. Flame* 81:50 (1990).
11. Deng, Z. T., Litchford, R., and Jeng, S. M., (1992) Rep. 92-3122, American Institute of Aeronautics and Astronautics (AIAA), Reston (VA), U.S.A.
12. Daou, J., and Haldenwang, P., *Eur. J. Mech. B* 16:141 (1997).
13. Patankar, S. V., *Numerical Heat Transfer and Fluid Flow*, Hemisphere, New York, 1980, p. 22.
14. Stüben, K., *Appl. Math. Comput*. 13:419 (1983).
15. Ruge, J., and Stüben, K., *The Institute of Mathematics and its Applications Conference Series*, New Series Number 3, (D. J. Paddon and H. Holstein, Eds.), Clarendon Press, Oxford, England, 1985, p. 169.
16. Levich, V. G., *Physicochemical Hydrodynamics*, Prentice-Hall, New York, 1962.
17. Clift, R., Grace, J. R., and Weber, M. E., *Bubbles, Drops and Particles*, Academic Press, New York, 1978.

Received 17 September 1996; accepted 18 November 1997